

Strain-induced Orientation Response of Endothelial Cells: Effect of Substratum Adhesiveness and Actin-myosin Contractile Level

Hai Ngu*, Lan Lu*, Sara J. Oswald*, Sarah Davis*, Sumona Nag* and Frank C-P Yin†

Abstract: Endothelial cells subjected to cyclic stretching change orientation so as to be aligned perpendicular to the direction of applied strain in a magnitude and time-dependent manner. Although this type of response is not the same as motility, it could be governed by motility-related factors such as substratum adhesiveness and actin-myosin contractile level. To examine this possibility, human aortic endothelial cells (HAEC) were uniaxially, cyclically stretched on silicone rubber membranes coated with various concentrations of fibronectin, collagen type IV and laminin to produce differing amounts of adhesiveness (measured using a radial flow detachment assay). Cells were subjected to 10% pure cyclic uniaxial stretching for three hours at a rate of 10%/sec. Time-lapse images revealed that cells underwent large morphological changes without moving. For each type of protein there was a parabolic dependence on initial adhesiveness with optimal cell orientation occurring at very similar adhesive strengths. The effect of actin-myosin contractile level was examined by stretching cells treated with different doses of 2,3-butanedione monoxime (BDM) and Blebbistatin. Each drug induced a dose-dependent decrease in orientation angles after three hours of cyclic stretching. Furthermore, cell and stress fiber orientations were tightly coupled for untreated and Blebbistatin-treated cells but were uncoupled for BDM-treated cells. Even though orientation response to cyclic stretching is not a spontaneous motile response, it is determined, in large part, by the same factors that affect spontaneous motil-

ity – the cell-substratum adhesiveness and actin-myosin contractile level.

Keyword: substratum adhesiveness, cell orientation, contractility, cyclic strain

1 Introduction

Situated on the inner lumen of blood vessels, endothelial cells are subjected to mechanical stimuli such as cyclic circumferential strain and pulsatile axial fluid shear stress. In response to fluid shear stress (FSS), cultured endothelial cells and their actin stress fibers (SFs) align parallel to the flow direction (1-3) and also reorganize their adhesion complexes (4, 5). FSS also accelerates wound closure (6) and affects gene and protein levels (7, 8). In contrast, endothelial cells respond to stretching by changing their orientations to be more or less perpendicular to the direction of applied strain (9). Stretching also redistributes integrins, reorganizes SFs and focal adhesions, and changes gene expression profile (5, 10-12). Recent findings demonstrate that these responses are not limited to cultured cells. SFs in endothelial cells of intact renal arteries subjected to four hours of longitudinal cyclic strain reoriented from their normal axial to the circumferential direction. This reorganization of the cytoskeleton was accompanied by loss of endothelium-dependent vasodilation (13). Taken together, this body of evidence suggests that, in addition to FSS, cyclic strain could also be an important determinant of endothelial cell morphology and function in vivo.

To date, the mechanisms underlying the orientation responses of endothelial cells to cyclic strain have not been characterized fully. It is likely that these responses may involve either morphological (i.e. shape changes with lamellipodial protrusion

* Department of Biomedical Engineering, Washington University in St. Louis, St. Louis, MO 63130

† Corresponding author. Washington University in St. Louis, Department of Biomedical Engineering, One Brookings Drive, Campus Box 1097, St. Louis, MO 63130, Phone: (314) 935-7177, Fax: (314) 935-7448, Email: yin@biomed.wustl.edu

sions and retractions) and/or more or less translation of the entire cell. Regardless, both of these possibilities have elements akin to spontaneous cell motility. Spontaneous cell motility involves the coordinated dynamic formation of new attachments to the underlying substratum at the leading edge, breakdown of bonds at the trailing edges and loosening of adhesions elsewhere. This complicated process involves both the actin cytoskeleton and focal adhesions and is affected by the surface density, expression and type of integrins on the cell surface interacting with various ligands on the substratum (14). Remarkably, it has previously been shown that cell attachment strength is a unifying mechanism underlying motility, regardless of the integrins that are involved with various extracellular matrix (ECM) proteins (14, 15). In these studies, both cell migration speed and spontaneous motility were optimum at similar attachment strengths of different ECM proteins. Furthermore, a recent study (16) demonstrated that cell motility induced by FSS is also dependent on adhesiveness. Hence both spontaneous and induced cell motility are dependent on cell-substratum attachment strength. Although endothelial cell orientation changes induced by mechanical stimuli are not what is normally considered to be motility, i.e. translocation, because many of the same structures, i.e. SFs, focal adhesions, and integrins are involved in both types of responses, it is possible that some of the same factors govern motility and mechanically-induced orientation.

Actin SFs play a critical role in controlling cell motility. In addition, many previous studies have shown that, when subjected to cyclic stretching, SFs as well as cell bodies oriented away from the stretching direction (17-19). SFs are the primary structures supporting intracellular tension and are dependent on actin-myosin contractile interactions. Blocking SF polymerization with cytochalasin B or markedly diminishing actin-myosin interaction with 2,3-butanedione monoxime (BDM) inhibited stress fiber remodeling and reorientation of endothelial cells subjected to cyclic stretching (17, 20). Thus, it is likely that cell orientation responses could also be modulated by decreasing

SF contractile activity.

How substratum adhesiveness and SF contractile levels affect cell orientation responses to cyclic stretching has not been examined in detail. If these responses are affected by these two factors in the same manner as spontaneous motility, this would be strong functional evidence for the commonality of these two types of responses. The studies described in this manuscript address this issue.

2 Materials and Methods

2.1 Membrane Preparation

Square (55 × 55 mm) silicone rubber membranes (Specialty Manufacturing, Saginaw, MI) were washed three times - twice in 70% ethanol and a final wash in phosphate-buffered saline (PBS). After drying, a 1 mL solution containing a specific concentration of one of three physiologically relevant ECM proteins (fibronectin, collagen IV, or laminin-10) (21-23) in PBS was allowed to cover a 1" diameter area located in the center of the membrane. The membrane was incubated with the protein solution overnight at 37°C. Unadsorbed proteins were aspirated and non-specific interactions were blocked using 1% sterile-filtered bovine serum albumin (BSA) for 20 minutes. The membrane was washed twice with PBS before cells were introduced and allowed to adhere onto the protein-coated surface.

2.2 Cell Culture

Human aortic endothelial cells (HAEC) from Clonetics (Walkersville, MD) at passages 9 to 14 were cultured in essential basic growth medium (EGM-2) with supplements and 2% fetal bovine serum. Cells were grown to semi-confluency on culture plates at 37°C inside an incubator with humidified air consisting of 5% CO₂. Cells were harvested using 0.05% trypsin/EDTA, centrifuged at 1000 rpm for 5 minutes, and resuspended in serum-free medium before adhering onto silicone rubber membranes coated with the desired concentration and type of ECM protein as described above. To avoid cell-cell interaction effects, cells were plated sparsely at a density of

~ 1000 cells/cm² to obtain a culture of predominantly individual cells devoid of contact with neighboring cells. Cells were allowed to attach and spread overnight at 37°C inside an incubator prior to study.

2.3 *Modulating Actin-myosin Contractility*

BDM and Blebbistatin are known to decrease nonmuscle cell actin-myosin contractile interactions. BDM is an inhibitor of the ATPase activity of muscle and nonmuscle myosin II (24-27). Blebbistatin has higher affinity and selectivity toward myosin II than BDM and has been shown to inhibit both ATPase and gliding motile activities of human platelet nonmuscle myosin II without perturbing myosin light chain kinase (28).

To examine the effect of modifying actin-myosin interaction, cells were pre-treated with 30 or 40mM BDM (Sigma-Aldrich, St. Louis, MO) or 5 or 10 μ M Blebbistatin (EMD Biosciences, La Jolla, CA) for 30 minutes prior to cyclic stretching and exposed continuously to the drug throughout the intervention.

2.4 *Cyclic Cell Stretching*

The cell stretching apparatus was described previously (29). After overnight incubation, the silicone rubber membranes with attached and spread cells were mounted onto the stretching apparatus located inside an incubator with a temperature setting of 37°C and humidified air consisting of 5% CO₂. The membranes were uniaxially stretched at a magnitude and rate of 10% and 10%/s, respectively, for different durations. At the end of the prescribed duration, the cells were fixed in 3.7% formaldehyde solution for 10 minutes. Cell images were acquired via phase contrast microscopy using a 10X objective. All experiments were repeated in triplicate for each experimental condition.

2.5 *Visualizing Actin Stress Fibers*

Formaldehyde-fixed cells were washed twice with PBS and permeabilized with a solution of 0.5% Triton X-100 for 3 minutes. Following three washes with PBS, nonspecific interactions were

blocked with 5% BSA solution for 20 minutes. The blocking solution was aspirated and cells were incubated with AlexaFluor Phalloidin (Invitrogen, Carlsbad, CA) at a 1:20 dilution in 1% BSA for 1 hour at ambient temperature. The sample was washed three times with 1% BSA followed by three washes with PBS. Samples were coverslipped with Fluoromount-G (Fisher Scientific, Houston, TX) and images were acquired using a digital camera mounted on a fluorescent microscope (Axioskop 2 MOT, Carl Zeiss, Thornwood, NY).

2.6 *Time-lapse Photomicroscopy*

To visualize the time course of orientation of live cells, we modified our previously described cell stretcher (30) so that it fit onto the stage of a phase-contrast light microscope. The microscope and stretcher were placed inside a 37°C incubator with 5% CO₂ humidified air. Silicone rubber membranes were coated with 10 μ g/mL fibronectin, as described above. After allowing cells to attach and spread overnight, membranes were subjected to 10% uniaxial cyclic strain at a rate of 10%/s for 3 hours. Real-time images, at approximately the maximum of the stretching cycle, were taken manually at 10 to 15 minutes intervals without interrupting the stretching.

2.7 *Image Analysis*

Measurements of cell orientation were made from the digitized images using Scion Image (Scion Corporation, MD) and quantified by the angle of the long axis of the cell relative to the stretching direction (defined as 0° and 180°). Because of symmetry about the axis orthogonal to the stretching direction, all orientation angles can be considered to be between 0 and 90°, inclusive. Only cells that did not contact any neighboring cells were analyzed. Measurements from pooled triplicate experiments (a total of approximately 1000-1300 cells) are reported for each experimental condition.

The relationship between cell and stress fiber orientation was determined using subsamples of ~ 50 cells for each experimental condition. For each of these cells, the orientation angles of all

Table 1: Comparison of semi-automatically estimated stress fiber orientations using different subregion sizes. Manual measurements are provided for comparison.

Analysis Type	Subregion pixel size	Cell A SF orientation (deg)	Cell B SF orientation (deg)
Manual	N/A	79.76	65.76
Semi-automated	20×20	80	66
	12×12	79	65
	40×40	80	66

SFs (defined in the same manner as cell orientation described above) were computed semi-automatically from digital fluorescent images with an algorithm written using Matlab (MathWorks, Natick MA). The algorithm is based on a previously published method (31, 32). In brief, the outline of the target cell was first drawn to exclude the perimeter of the cell so that only the enclosed SFs were analyzed. The cell interior was divided into subregions of 20×20 pixel size. For each subregion, a pixel-by-pixel intensity gradient perpendicular to the local SF direction was first calculated and expressed as magnitude and direction. To determine the dominant direction for this subregion, accumulator bin values for the possible orientations of 0 to 179° were calculated by summing a weighted contribution from each pixel. The orientation with the largest bin value was then determined as the dominant direction and converted into the range from 0 to 90° to be consistent with our cell angle measurements. For each subregion, the resultant orientation was represented by a line. To eliminate the effect of the subregions that did not contain any SFs, a threshold value was set for the intensity of each subregion and only the regions with intensities exceeding the threshold were processed. The angles of the lines for all subregions containing a SF were tabulated and the median value was considered to represent the orientation of the SFs of that cell. Figure 1 shows an illustrative example of the raw image of the SFs and the superimposed lines from representative subregions. The accuracy and robustness of this algorithm were examined by first verifying that the SF orientation was the same for subregions both larger and smaller than the intermediate-sized one we used for experimental analysis. The results shown in Table

1 verify that the resulting SF orientation does not depend on the size of the subregion. Comparison of the results of the algorithm with those obtained by manual measurements of the orientations of the same SFs of two arbitrarily selected cells are also shown in Table 1. There was no significant difference between the manually and semi-automatically estimated orientations.

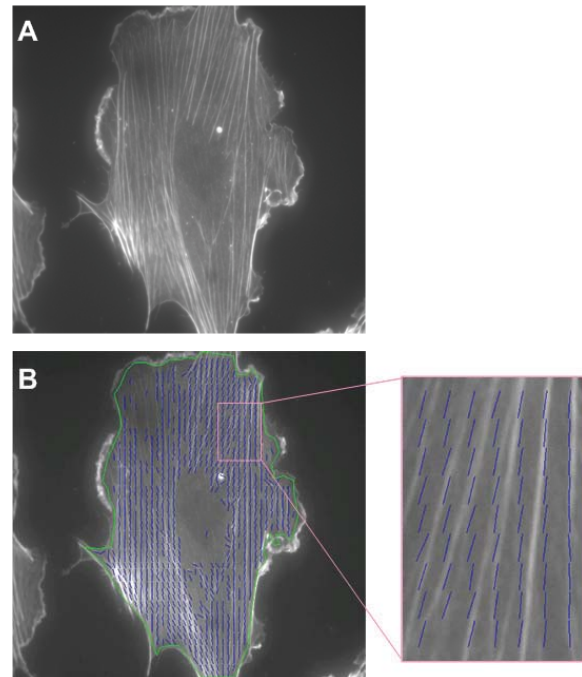


Figure 1: Semi-automated measurement of stress fiber orientation in a cell. Fluorescent image of actin stress fibers in a representative cell (A). Same image as in panel (A) shown with overlaid computer-generated orientation lines (B). The inset is a magnified view of one region.

2.8 Measuring Cell Attachment Strength

Cell attachment strength was assessed using a radial flow detachment assay (RFDA) (33-36). Briefly, fluid was introduced via an inlet tube (2mm diameter) located at the top center of two transparent parallel circular plates. The flow was driven by a specially-designed, adjustable pressurized fluid reservoir and volumetric flow rate was monitored by a flow meter. Firmly attached to the bottom plate was an ECM protein-coated circular silicone rubber membrane (2.54 cm diameter) with adherent cells. The separation distance between the surface of the membrane and the top plate (maintained by four high precision spacers) for all studies was 200 μ m. Fluid flowing radially outward and exiting at the periphery, induced FSS that varied inversely with radial position. By selecting different flow rates (by changing the pressure) and/or fluid viscosities (by adding high molecular weight dextran to PBS), a wide range of FSS could be obtained.

Cells were attached for 10 minutes following which images of arbitrarily selected regions were captured using phase-contrast microscopy and a 10X objective lens to determine initial cell density. The radial flow chamber was carefully assembled and fluid flow was initiated by opening a one-way valve after 15 minutes of total attachment time for all experiments. Cells were sheared for 15 minutes at ambient temperature. All adhesive strength experiments were repeated at least in triplicate.

At the end of the experiment the cells were fixed in 3.7% formaldehyde in PBS for 10 minutes. Serial images along two mutually perpendicular diameters were taken. The average number of adherent cells at each radial position was obtained using NIH Image. The critical radial position (R_c) corresponding to 50% cell detachment was determined by fitting the data to a sigmoidal logistic curve:

$$f(r) = \frac{1}{1 + e^{\frac{-(r-R_c)}{b}}}$$

where f is the fraction of adherent cells, r is radial position, and b is a constant that depends upon the shape of the curve. The criteria that $R_c > R_{\min}$ (the

minimal radial position, see Section 3.2 of Results) was satisfied for all experiments. The estimated FSS corresponding to R_c is called the critical FSS and is the measure of attachment strength. It was estimated using the creeping flow assumption with power series expansion correction (37, 38):

$$\tau_w = \left| \frac{3\mu Q}{\pi h^2 r} - \frac{3\rho Q^2}{70\pi^2 h r^3} \right|$$

where τ_w is wall shear stress, h is separation distance, μ and ρ are fluid viscosity and density, Q is volumetric flow rate, and r is radial position. Both inlet and local Reynolds numbers were computed to ascertain that the flows were laminar ($Re < 2000$) so that the above estimation can be used:

$$Re_{inlet} = \frac{2\rho Q}{\pi\mu R_i}$$

$$Re_{local} = \frac{\rho Q}{\pi\mu r}$$

where R_i is inlet radius and the other variables are as noted above.

2.9 Modeling Wall Shear Stress

Depending on flow conditions, the RFDA chamber has a variable-sized stagnation region at its center. We used the computational fluid dynamics (CFD) software FLUENT and GAMBIT (Fluent Inc, Lebanon, NH) to simulate the flow profile throughout the chamber, including the stagnation region. The 2D axisymmetric model consisted of a central inlet with a 1mm radius and two parallel plates separated by 200 μ m. Fluid flow entered axially from the inlet, impinged onto the bottom surface, and exited radially between the plates. A parabolic velocity profile was used for the inlet flow and no-slip conditions were imposed on all solid boundaries. Simulations were made using a density of 1 g/cm³ for a variety of fluid viscosities and inlet flow rates to cover a range of inlet Reynolds numbers. In all cases, we used a convergence criterion of 10⁻⁶.

2.10 Statistical Analysis

Because cell and SF orientation angles do not have Gaussian distributions, we reported the results in terms of median values and performed statistical comparisons using the nonparametric Kruskal-Wallis test. We made post-hoc multiple pairwise comparisons using Dunn's method and inferred a statistically significant difference for $p < 0.05$.

3 Results

3.1 Effect of ECM Protein Concentration on Cell Orientation Angles

Figure 2 consists of time-lapse images of a group of cells on fibronectin-coated membranes after various durations of stretching. The responses of the two extremes of initially elongated cells are highlighted. Cells initially aligned oblique to the stretching direction do not change orientation nor seem to have any discernible response. In contrast, the cell initially aligned nearly parallel to the stretching direction rounds up and then elongates in the direction perpendicular to the stretching direction. Most, but not all, of the initially round cells also elongate and eventually end up being aligned perpendicular to the stretching direction. Note that none of the cells appear to move.

Figure 3A-C summarizes the cell orientation angles as a function of protein coating concentration for each of the different ECM proteins after three hours of cyclic stretch. For each type of protein, there is a parabolic dependence of cell orientation on concentration with the maximal responses occurring at widely different concentrations ranging from 3.5 to 20 $\mu\text{g}/\text{mL}$ for the three proteins.

3.2 Modeling Wall Shear Stress

Typical simulated results of wall shear stress in the assay chamber are shown in Figure 4A. In particular, the position corresponding to the radius where the difference between the simulated and calculated τ_w becomes less than 5% is demarcated. This radial position is referred to as the minimal radial position (R_{\min}). Since the measurement of cell attachment strengths requires

manipulating the flow-related variables, these minimal radial positions for different Reynolds numbers must be determined via additional CFD simulations. The results of these simulations for Reynolds numbers spanning the entire laminar regime are shown in Figure 4B. As the Reynolds number increases, inlet inertial effects become more significant and the minimal radial position (R_{\min}) in which τ_w is accurate increases (37). There is a linear relationship between minimal radial position and inlet Reynolds number. Further CFD simulations show that geometric sizing effects can affect the laminarity of fluid flow (data not shown). Taken together, these results highlight the importance of conducting a thorough computational investigation before making experimental measurements.

3.3 Effect of Adhesive Strength on Cell Orientation

Figure 5A-C shows that cell-substratum adhesive strength increases as a function of protein concentration. The plateau in adhesive strength at high concentrations signifies saturation of the surface. Panel D illustrates the parabolic dependence of cell angle on adhesive strength. Unlike the widely different concentrations of individual proteins that produce the maximal response, the adhesiveness corresponding to the maximum cell orientation response is similar for all three ECM proteins. This suggests that substratum adhesiveness is the likely mechanism underlying this response.

3.4 Effect of Actin-Myosin Contractile Level on Cell and SF Orientations

Figure 6 summarizes the interdependence of cell orientation angle on stretching duration and actin-myosin contractile level. For all three groups cell orientation angles increased with duration and both BDM and Blebbistatin produced blunted, dose-dependent responses at longer durations.

Representative fluorescent images (Figure 7) show that drug treatment does not affect the integrity or density of actin stress fibers. Regular arrays of stress fibers are visible for both control and drug-treated cells subjected to cyclic stretching. The orientations of the cell and its stress fibers

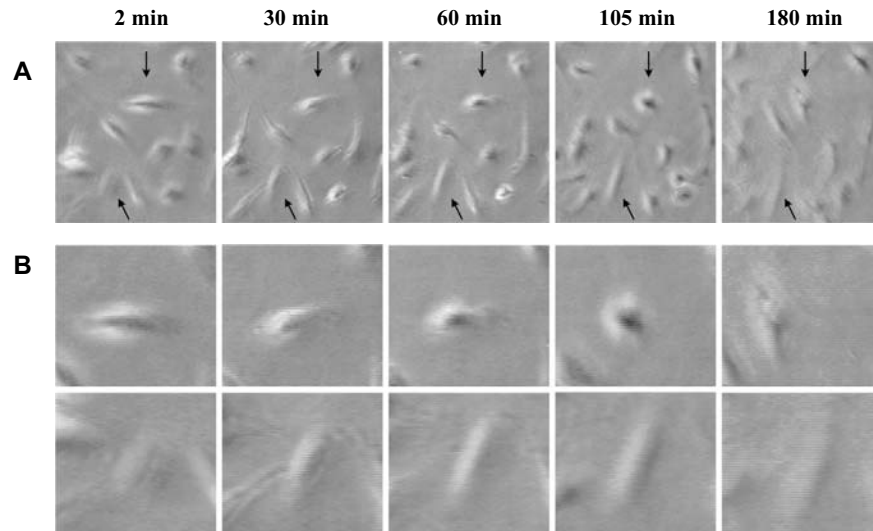


Figure 2: (A) Time-lapse images of a group of cells at various times after the onset of cyclic stretching in the horizontal direction. (B) Magnified views of two selected cells of interest (depicted by the arrows in panel A).

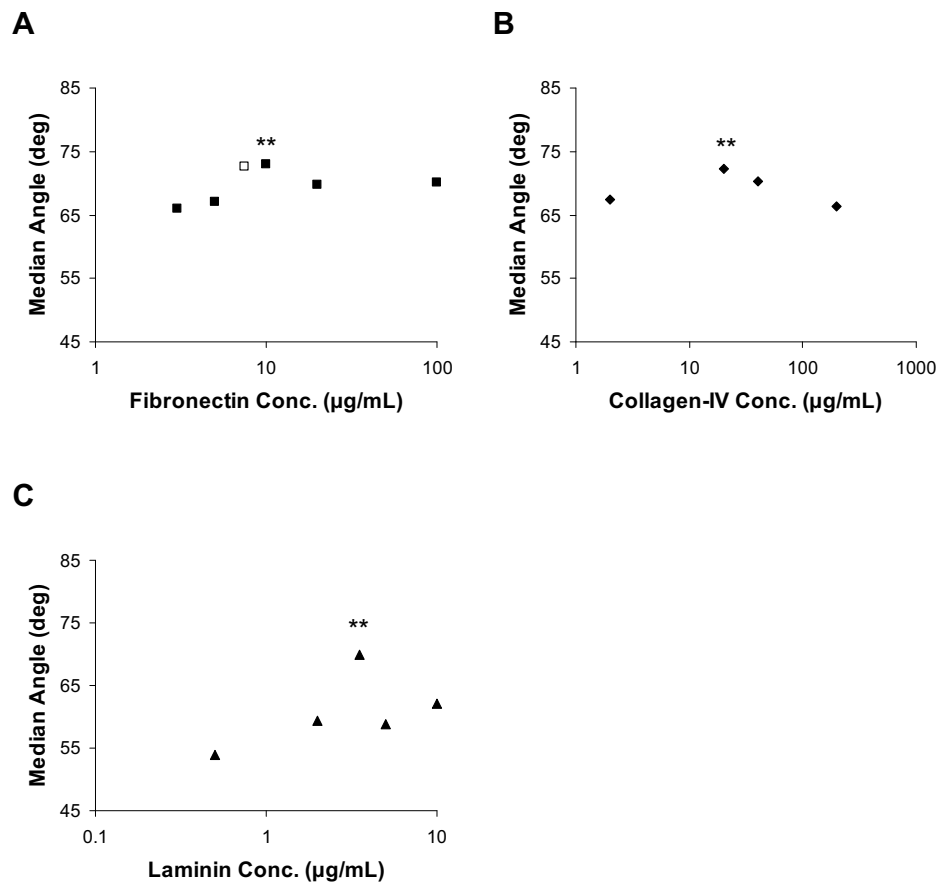
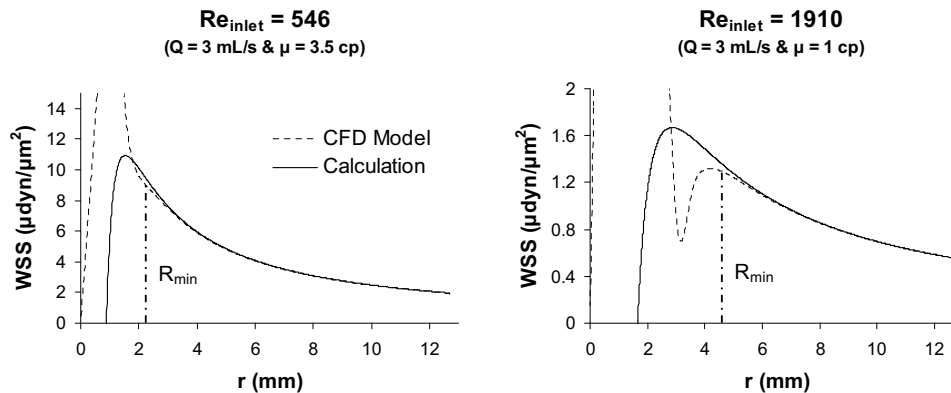


Figure 3: Sensitivity of cell orientation response to different ECM protein coating concentrations. Membranes were subjected to cyclic strain at a magnitude, rate and duration of 10%, 10%/s and 3hrs, respectively on membranes coated with (A) fibronectin, (B) collagen type IV and (C) laminin. **denotes the maximum response. All pairwise comparisons involving the maximum response were statistically significant except for the pair involving the open symbol.

A



B

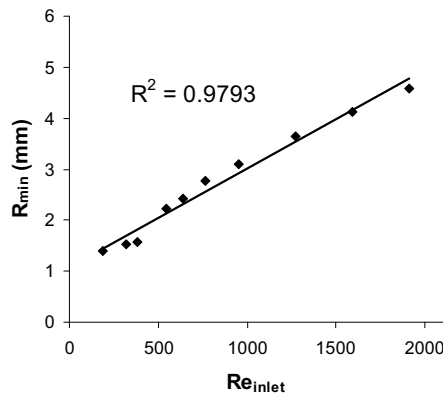


Figure 4: Computational modeling of wall shear stress (WSS). (A) Shift in R_{\min} as Reynolds number increases, (B) plot of R_{\min} versus inlet Reynolds number.

are very similar for control and Blebbistatin-treated cells. However, discernible differences in cell and stress fiber orientations are observed for the BDM-treated cell. Needle-like projections of the stress fibers pushing the cell membrane outwards are clearly visible for the BDM-treated cells. Summary cell and stress fiber orientation data are shown in Figure 8. Cell body and stress fiber angles are tightly coupled for control and Blebbistatin-treated cells whereas they are uncoupled for BDM-treated cells after two or more hours of stretching. To investigate whether this uncoupling response from BDM-treated cells is due to a possible effect of the drugs on cell adhesion, the adhesive strengths of control, Blebbistatin and BDM-treated cells were measured and found not to be significantly different (data not

shown).

4 Discussion

Cell motility involves the coordinated making and breaking of sufficient numbers of bonds between the cell and the substratum to enable the cell body to translocate to a new position. In contrast, cell orientation response to cyclic stretching does not produce translation of the cell body. Rather, the making and breaking of the bonds appears to result predominantly, if not exclusively, in large morphological changes that are manifested as a change in alignment. In fact, there appears to be sufficient residual adhesion between the cell and substrate that it is not detached during the stretching intervention. In that sense, it is not a classic motile response. Regardless of what one calls this

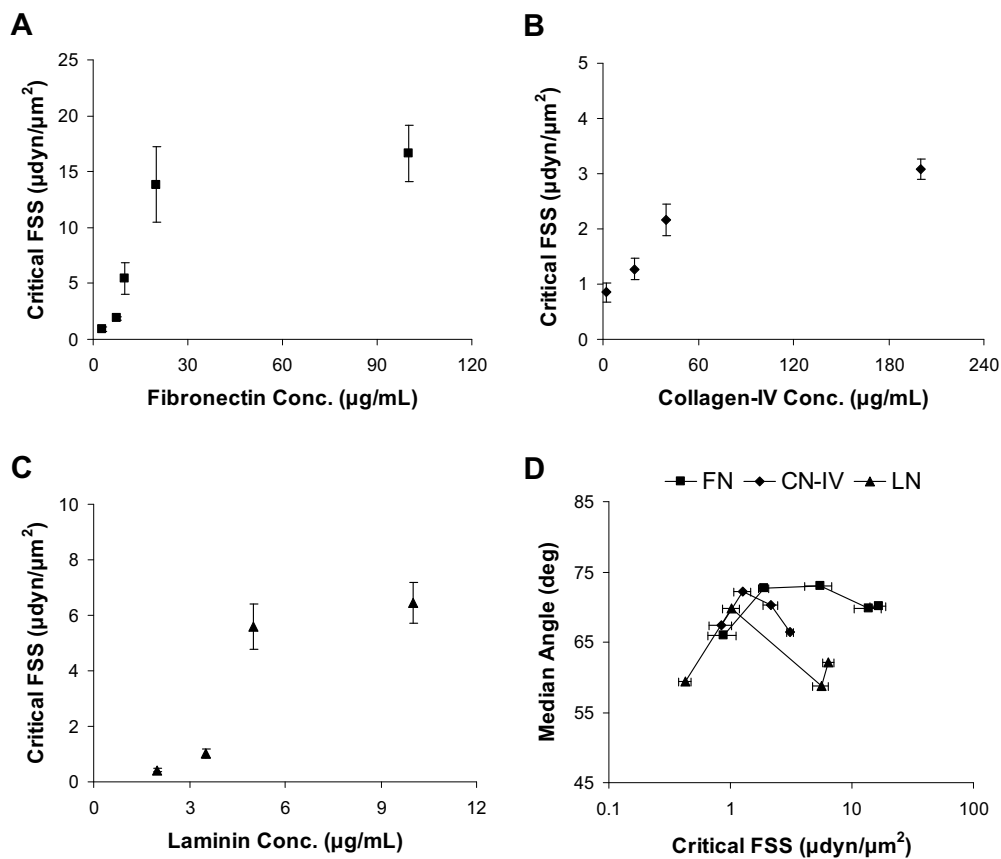


Figure 5: Effect of substratum adhesiveness on endothelial cell orientation response. Critical FSS (mean \pm stdev) as a function of protein coating concentration for (A) fibronectin (FN), (B) collagen Type IV (CN-IV) and (C) laminin (LN). Median cell angles as a function of adhesive strength corresponding to panels A-C and Figure 3 (D). Because the statistical significance of the responses relative to the maximum are the same as those depicted in Figure 3 they are not repeated in this figure.

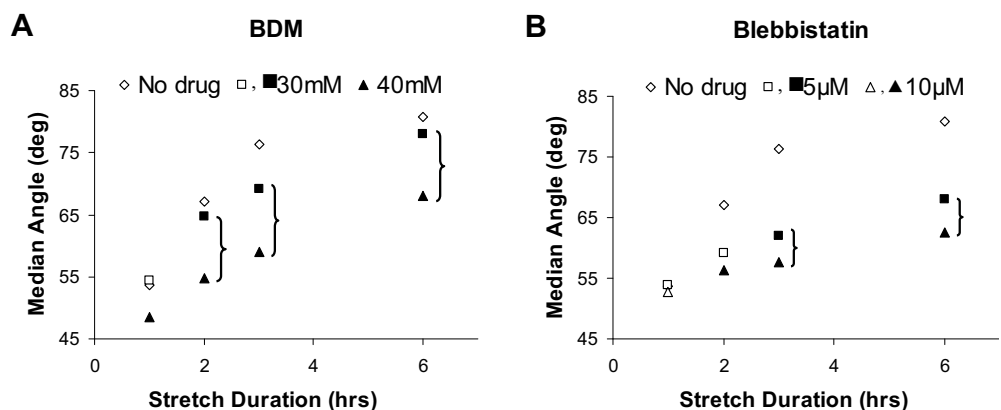


Figure 6: The effect of actin-myosin contractile level on endothelial cell orientation in response to cyclic stretching. A strain magnitude and rate of 10% and 10%/s, respectively, were applied to membranes coated with 10 $\mu\text{g/mL}$ fibronectin. Filled symbols denote significant differences from control (no drug) values at each stretch duration. The brackets denote significantly different effects of the drug concentrations.

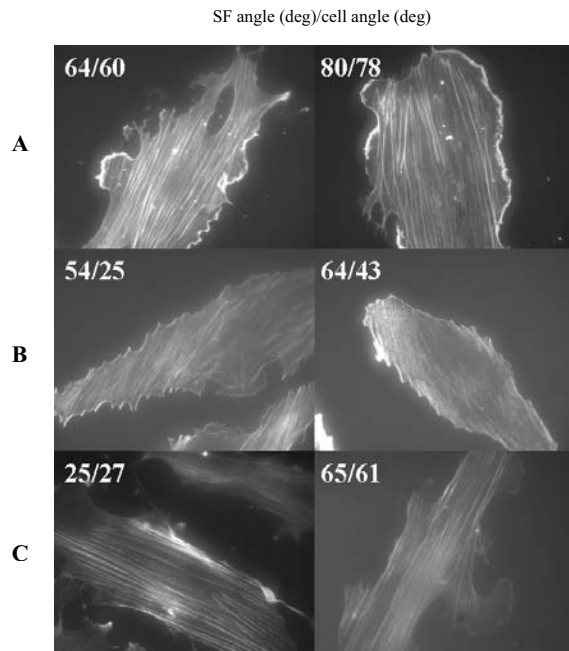


Figure 7: Representative images of cell and stress fiber orientation after 3 hours of cyclic stretching in the horizontal direction. (A) control untreated, (B) 40mM BDM treated, and (C) 10 μ M Blebbistatin treated cells. A strain magnitude and rate of 10% and 10%/s, respectively, were applied to membranes coated with 10 μ g/mL fibronectin. Individual cell and stress fiber angles are listed with each image.

response, the results of the present study support the notion that mechanically-induced cell orientation responses share many features in common with spontaneous motility. Several aspects of this study deserve further discussion.

First, like motility, the cell orientation response, has a parabolic dependence on attachment strength. The optimum response occurs at nearly the same attachment strength regardless of the type of ECM protein with which the cell interacts. The following scenario could explain this observation. At low adhesiveness there are likely insufficient attachments to the substratum to enable adequate traction forces to change shape. At high adhesiveness there could be an overabundance of attachments that impede cell shape change. It is not yet known whether the high attachment state produces a “stop” signal for shape change as has

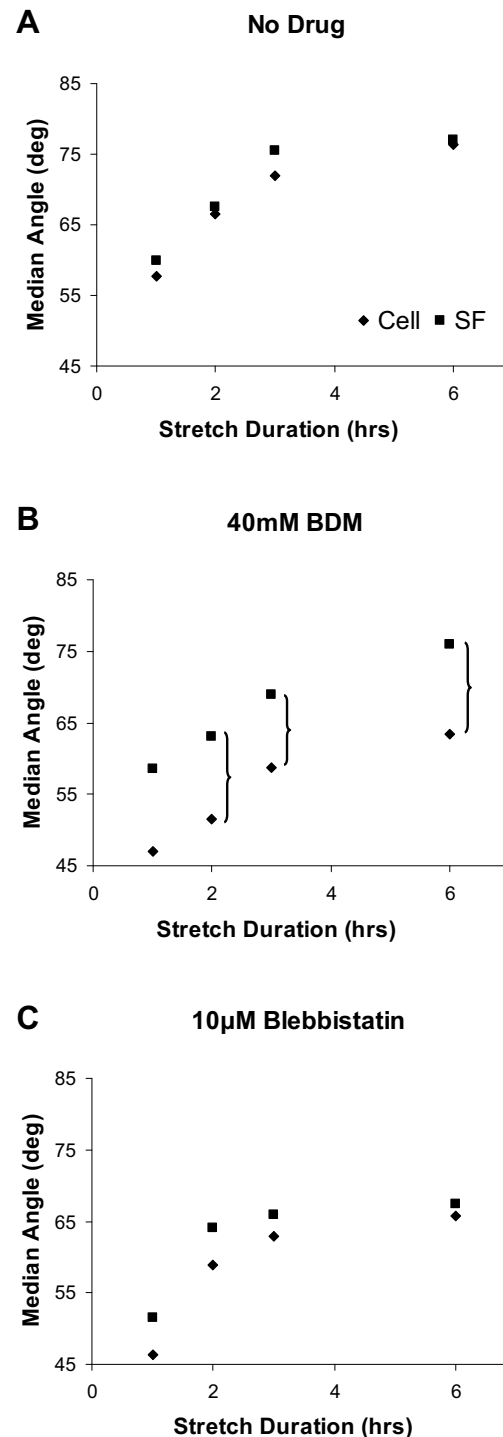


Figure 8: Cell and stress fiber orientations. Cells were either untreated (A) or treated with 40mM BDM (B) or 10 μ M Blebbistatin (C). A strain magnitude and rate of 10% and 10%/s, respectively, were applied to membranes coated with 10 μ g/mL fibronectin. Brackets denote significant differences between the cell body and SF responses.

recently been reported for motility (39). Regardless, optimal cell orientation responses require a fine balance between the number of adhesive bonds and traction forces.

Second, as the time-lapse images show, at least some cells undergo a dramatic shape change as part of the orientation response. Cells initially aligned along the stretching direction appear to round up and then elongate obliquely to the stretching direction. Our observations are consistent with a previous study which also reported that cells initially aligned parallel with the stretch direction underwent drastic morphological changes consisting of initial rounding followed by elongation in the direction orthogonal to that of the mechanical stimulus (40). Our observations were made without interrupting the stretching whereas the previous study interrupted the stretching every few minutes. Nevertheless, the similarity of the findings suggests that morphological changes are the major feature of this mechanically-induced response. Even though the specific details of how this orientation is achieved have yet to be elucidated, it is likely that the rounding up requires loosening and/or breakage of many attachments to the substrate. Hence, at certain times after the onset of stretching, the cell state could resemble the initial binding to the substratum. Furthermore, it has been shown that within 15 minutes of initial binding, partial but not complete assembly of cytoskeletal proteins may be present (41). These findings could explain the dependence of the orientation response of the cell body on initial cell-substratum adhesive strength. The subsequent elongation requires the formation of new attachments allowing the cell to polarize and protrude its membrane and cytoskeleton in a particular direction but is different than spontaneous motility because the cell does not move.

Third, the properties of the substrate (adhesiveness, stiffness, etc.) are clearly important in regulating cell motility. The internal forces that a cell can generate are supported by actin SFs (42) with the amount transferred to the substrate, i.e. the traction forces, dependent upon its stiffness relative to that of the cell. Our results showing that orientation responses are affected by decreasing

actin-myosin contractile level (and thereby traction forces) in a dose-dependent manner underscore the importance of traction forces in modulating these responses. In fact, we recently demonstrated directly that decreasing contractility decreased the internal loading of cells (43). This dependence on internal tension could also explain why cells initially aligned obliquely to the stretching direction do not respond. Such cells likely are already predominantly internally loaded in that direction. If so, stretching in the orthogonal direction may also not produce a sufficiently large stimulus to cause an orientation response.

Fourth, when endothelial cells are subjected to cyclic strain, focal adhesion complexes remodel, the entire cytoskeleton appears to completely break down, and then reorganizes into parallel arrays perpendicular to the stretch direction (5, 11, 12, 44). These findings indirectly suggest that the orientation response does not necessarily require a completely intact cytoskeleton. Our results directly demonstrate that under some conditions the cell body and SF responses are not coupled. Unlike the tight coupling between cell body and SF responses in normal and Blebbistatin treated cells, BDM caused significant differences in cell and SF orientation responses. This uncoupling between cell body and SF responses may be caused by nonspecific effects induced by the drug since Blebbistatin is a specific inhibitor of myosin-II. For example, BDM has been found to delocalize actin leading edge proteins (45) and alter the activities of gap junctions (46) and potassium and calcium channels (47-49). It is noteworthy that uncoupling between cell body and SF responses to cyclic stretching was also observed in cells treated with an inhibitor of stretch-activated calcium channels (40). Regardless, the fact that the cell body and SF responses can be uncoupled illustrates that SF reorganization is necessary but not sufficient for cell body reorientation. Further detailed study of the conditions and mechanisms underlying this finding is certainly warranted.

Acknowledgement: This research was supported by a grant-in-aid from the American Heart Association.

References

1. Dieterich, P., Odenthal-Schnittler, M., Mrowietz, C., Kramer, M., Sasse, L., Oberleithner, H. & Schnittler, H. J. (2000) *Biophys J* **79**, 1285-97.
2. Eskin, S. G., Ives, C. L., McIntire, L. V. & Navarro, L. T. (1984) *Microvasc Res* **28**, 87-94.
3. Girard, P. R. & Nerem, R. M. (1995) *J Cell Physiol* **163**, 179-93.
4. McCue, S., Noria, S. & Langille, B. L. (2004) *Trends Cardiovasc Med* **14**, 143-51.
5. Shikata, Y., Rios, A., Kawkitinarong, K., DePaola, N., Garcia, J. G. & Birukov, K. G. (2005) *Exp Cell Res* **304**, 40-9.
6. Albuquerque, M. L., Waters, C. M., Savla, U., Schnaper, H. W. & Flozak, A. S. (2000) *Am J Physiol Heart Circ Physiol* **279**, H293-302.
7. Hochleitner, B. W., Hochleitner, E. O., Obrist, P., Eberl, T., Amberger, A., Xu, Q., Margreiter, R. & Wick, G. (2000) *Arterioscler Thromb Vasc Biol* **20**, 617-23.
8. McCormick, S. M., Eskin, S. G., McIntire, L. V., Teng, C. L., Lu, C. M., Russell, C. G. & Chittur, K. K. (2001) *Proc Natl Acad Sci U S A* **98**, 8955-60.
9. Moretti, M., Prina-Mello, A., Reid, A. J., Barron, V. & Prendergast, P. J. (2004) *J Mater Sci Mater Med* **15**, 1159-64.
10. Feng, Y., Yang, J. H., Huang, H., Kennedy, S. P., Turi, T. G., Thompson, J. F., Libby, P. & Lee, R. T. (1999) *Circ Res* **85**, 1118-23.
11. Yano, Y., Geibel, J. & Sumpio, B. E. (1997) *J Cell Biochem* **64**, 505-13.
12. Yoshigi, M., Hoffman, L. M., Jensen, C. C., Yost, H. J. & Beckerle, M. C. (2005) *J Cell Biol* **171**, 209-15.
13. Sipkema, P., van der Linden, P. J., Westerhof, N. & Yin, F. C. (2003) *J Biomech* **36**, 653-9.
14. Palecek, S. P., Loftus, J. C., Ginsberg, M. H., Lauffenburger, D. A. & Horwitz, A. F. (1997) *Nature* **385**, 537-40.
15. DiMilla, P. A., Stone, J. A., Quinn, J. A., Albelda, S. M. & Lauffenburger, D. A. (1993) *J Cell Biol* **122**, 729-37.
16. Shiu, Y. T., Li, S., Marganski, W. A., Usami, S., Schwartz, M. A., Wang, Y. L., Dembo, M. & Chien, S. (2004) *Biophys J* **86**, 2558-65.
17. Iba, T. & Sumpio, B. E. (1991) *Microvasc Res* **42**, 245-54.
18. Takemasa, T., Sugimoto, K. & Yamashita, K. (1997) *Exp Cell Res* **230**, 407-10.
19. Zhao, S., Suciu, A., Ziegler, T., Moore, J. E., Jr., Burki, E., Meister, J. J. & Brunner, H. R. (1995) *Arterioscler Thromb Vasc Biol* **15**, 1781-6.
20. Wang, J. H., Goldschmidt-Clermont, P. & Yin, F. C. (2000) *Ann Biomed Eng* **28**, 1165-71.
21. Grant, D. S. & Leblond, C. P. (1988) *J Histochem Cytochem* **36**, 271-83.
22. Palotie, A., Tryggvason, K., Peltonen, L. & Seppa, H. (1983) *Lab Invest* **49**, 362-70.
23. Laurie, G. W., Leblond, C. P. & Martin, G. R. (1982) *J Cell Biol* **95**, 340-4.
24. Herrmann, C., Wray, J., Travers, F. & Barman, T. (1992) *Biochemistry* **31**, 12227-32.
25. Higuchi, H. & Takemori, S. (1989) *J Biochem (Tokyo)* **105**, 638-43.
26. McKillop, D. F., Fortune, N. S., Ranatunga, K. W. & Geeves, M. A. (1994) *J Muscle Res Cell Motil* **15**, 309-18.
27. Cramer, L. P. & Mitchison, T. J. (1995) *J Cell Biol* **131**, 179-89.
28. Straight, A. F., Cheung, A., Limouze, J., Chen, I., Westwood, N. J., Sellers, J. R. & Mitchison, T. J. (2003) *Science* **299**, 1743-7.

29. Wille, J. J., Ambrosi, C. M. & Yin, F. C. (2004) *J Biomech Eng* **126**, 545-51.
30. Owatverot, T. B., Oswald, S. J., Chen, Y., Wille, J. J. & Yin, F. C. (2005) *J Biomech Eng* **127**, 374-82.
31. Karlson, W. J., Covell, J. W., McCulloch, A. D., Hunter, J. J. & Omens, J. H. (1998) *Anat Rec* **252**, 612-25.
32. Karlson, W. J., Hsu, P. P., Li, S., Chien, S., McCulloch, A. D. & Omens, J. H. (1999) *Ann Biomed Eng* **27**, 712-20.
33. Peel, M. M. & DiMilla, P. A. (1999) *Ann Biomed Eng* **27**, 236-46.
34. Cozens-Roberts, C., Quinn, J. A. & Lauffenberger, D. A. (1990) *Biophys J* **58**, 107-25.
35. Tan, J., Shen, H. & Saltzman, W. M. (2001) *Biophys J* **81**, 2569-79.
36. Yung, L. Y., Colman, R. W. & Cooper, S. L. (1999) *Blood* **94**, 2716-24.
37. Goldstein, A. S. & DiMilla, P. A. (1997) *Biotech & Bioeng* **55**, 616-629.
38. Goldstein, A. S. & DiMilla, P. A. (1998) *AIChE J* **44**, 465-473.
39. Cox, E. A., Sastry, S. K. & Huttenlocher, A. (2001) *Mol Biol Cell* **12**, 265-77.
40. Hayakawa, K., Sato, N. & Obinata, T. (2001) *Exp Cell Res* **268**, 104-14.
41. Lotz, M. M., Burdsal, C. A., Erickson, H. P. & McClay, D. R. (1989) *J Cell Biol* **109**, 1795-805.
42. Pourati, J., Maniotis, A., Spiegel, D., Schaffer, J. L., Butler, J. P., Fredberg, J. J., Ingber, D. E., Stamenovic, D. & Wang, N. (1998) *Am J Physiol* **274**, C1283-9.
43. Lu, L., Feng, Y., Hucker, W. J., Oswald, S. J., Longmore, G. D. & Yin, F. C. P. (2008) *Cell Motil Cytoskeleton*, (in press).
44. Wang, J. H., Goldschmidt-Clermont, P., Moldovan, N. & Yin, F. C. (2000) *Cell Motil Cytoskeleton* **46**, 137-45.
45. Yarrow, J. C., Lechler, T., Li, R. & Mitchison, T. J. (2003) *BMC Cell Biol* **4**, 5.
46. Verrecchia, F. & Herve, J. C. (1997) *Am J Physiol* **272**, C875-85.
47. Schlichter, L. C., Pahapill, P. A. & Chung, I. (1992) *J Pharmacol Exp Ther* **261**, 438-46.
48. Ferreira, G., Artigas, P., Pizarro, G. & Brum, G. (1997) *J Mol Cell Cardiol* **29**, 777-87.
49. Lang, R. J. & Paul, R. J. (1991) *J Physiol* **433**, 1-24.

